Electronic Supplementary Information (ESI)

Triboelectrification of nanocomposites using identical polymer matrixes with different concentrations of nanoparticle fillers

Linards Lapčinskis,[1,2] Artis Linarts,[2] Kaspars Mālnieks,[1] Hyunseung Kim,[3,4] Kristaps Rubenis,[5] Kaspars Pudzs,[6] Krisjanis Smits,[6] Andrejs Kovaļovs,[7] Kaspars Kalniņš,[7] Aile Tamm,[8] Chang Kyu Jeong,[3,4]* Andris Šutka,[1]*

[1] Research Laboratory of Functional Materials Technologies, Faculty of Materials Science and Applied Chemistry, Riga Technical University, Paula Valdena 3/7, Riga, LV-1048, Latvia. E-mail: andris.sutka@rtu.lv

[2] Institute of Technical Physics, Faculty of Materials Science and Applied Chemistry, Riga Technical University, Paula Valdena 3/7, Riga, LV-1048, Latvia

[3] Division of Advanced Materials Engineering, Jeonbuk National University, Jeonju, Jeonbuk, 54896, Republic of Korea, E-mail: ckyu@jbnu.ac.kr

[4] Department of Energy Storage/Conversion Engineering of Graduate School & Hydrogen and Fuel Cell Research Center, Jeonbuk National University, Jeonju, Jeonbuk, 54896, Republic of Korea

[5] Rudolfs Cimdins Riga Biomaterials Innovations and Development Centre of RTU, Institute of General Chemical Engineering, Faculty of Materials Science, Riga Technical University, Pulka 3, Riga, LV-1007, Latvia

[6] Institute of Solid State Physics, University of Latvia, Kengaraga 8, Riga, LV-1063, Latvia

[7] Institute of Materials and Structures, Faculty of Civil Engineering, Riga Technical University, Kipsalas 6A, Riga, LV-1048, Latvia

[8] Institute of Physics, University of Tartu, W. Ostwaldi Street 1, 50411 Tartu, Estonia
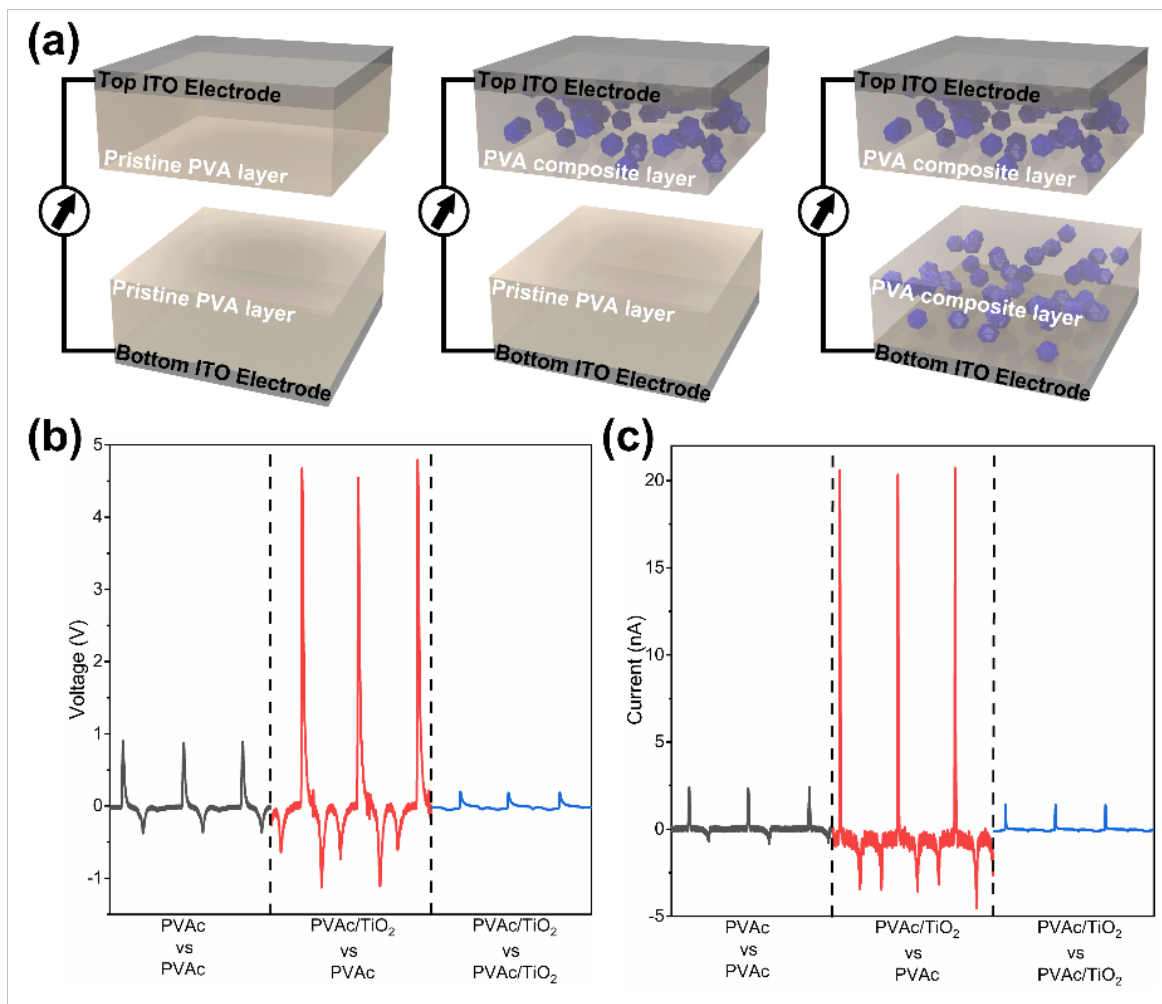
Fig. S1. (a) PVAc-based TEG devices. (b) Open-circuit voltage and (c) short-circuit current peaks of TEG devices constructed using either pristine PVAc or PVAc/TiO$_2$ (5 vol%) composite layers.
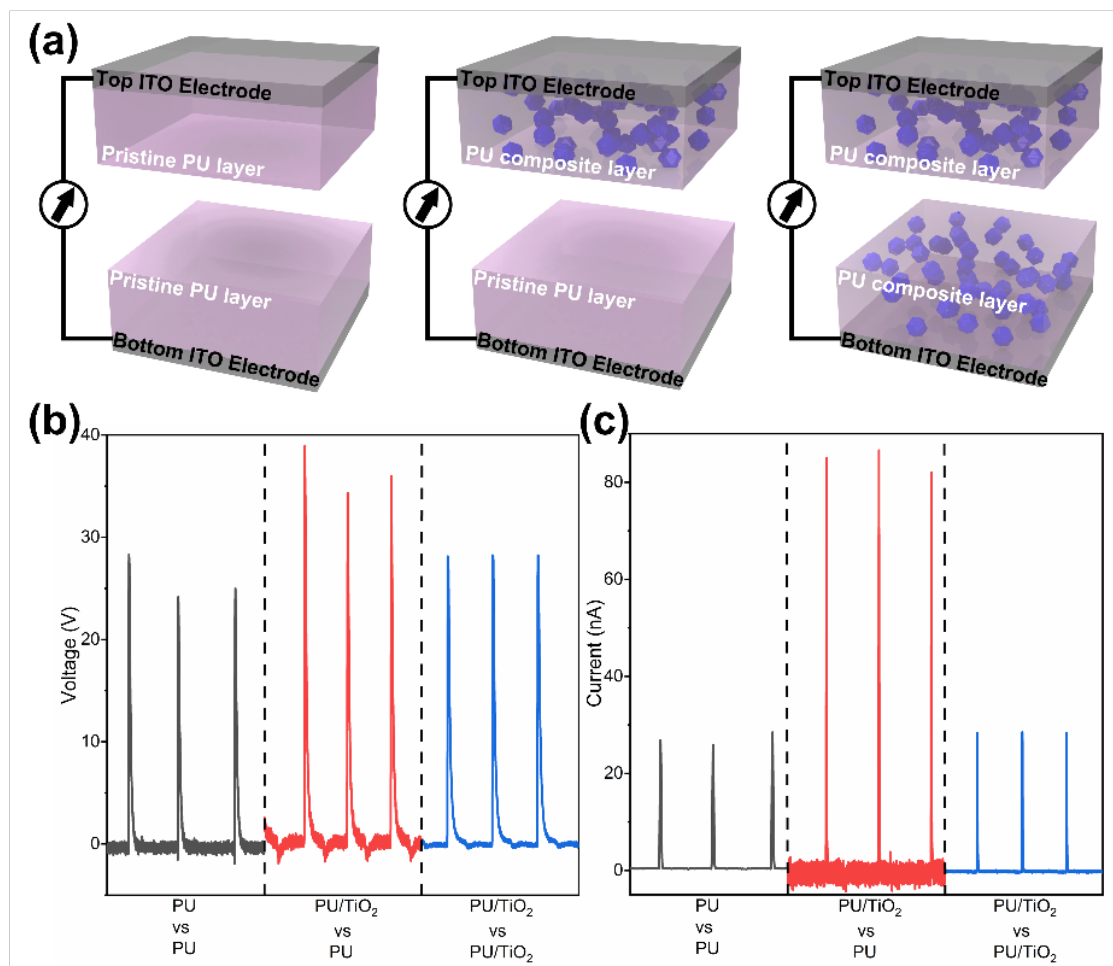
Fig. S2. (a) PU-based TEG devices. (b) Open-circuit voltage and (c) short-circuit current peaks of TEG devices constructed using either pristine PU or PU/TiO$_2$ (5 vol%) composite layers.
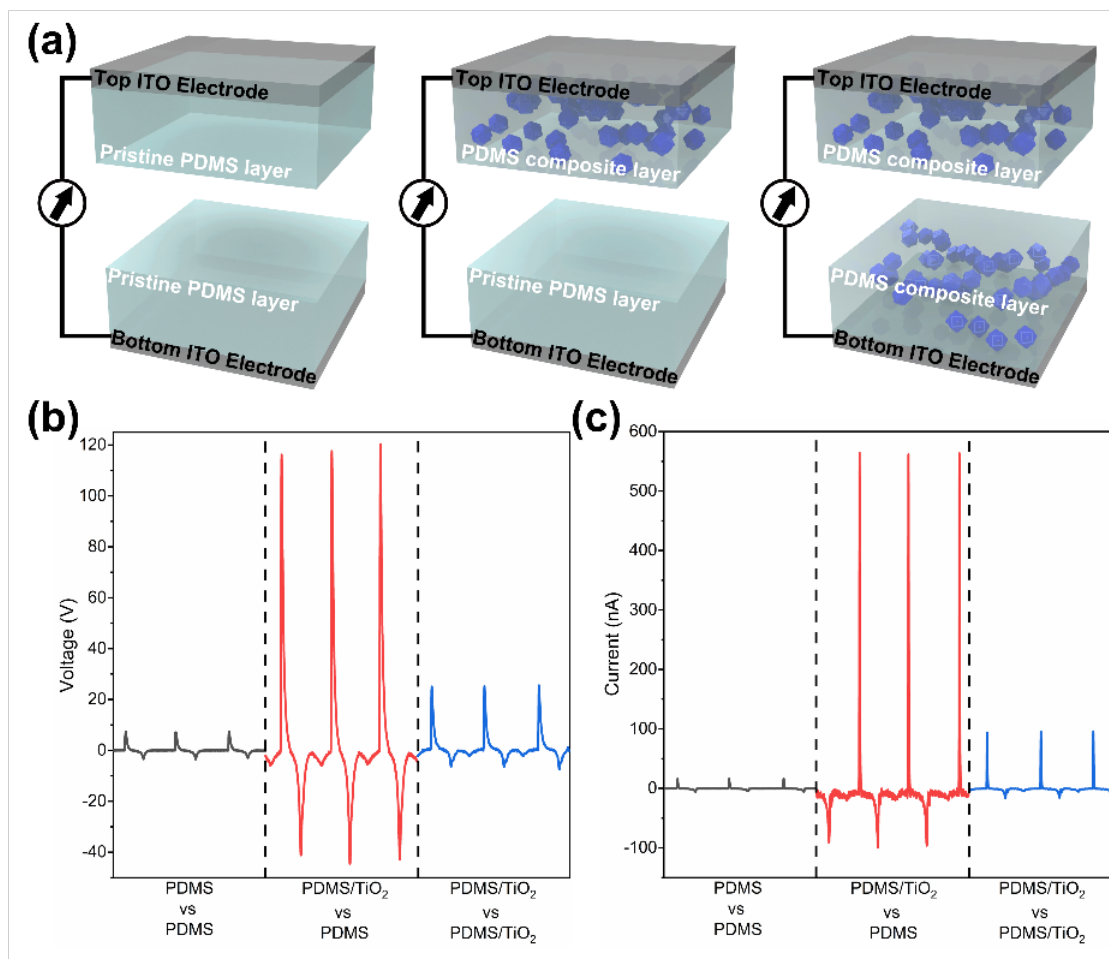
Fig. S3. (a) PDMS-based TEG devices. (b) Open-circuit voltage and (c) short-circuit current peaks of TEG devices constructed using either pristine PDMS or PDMS/TiO$_2$ (5 vol%) composite layers.
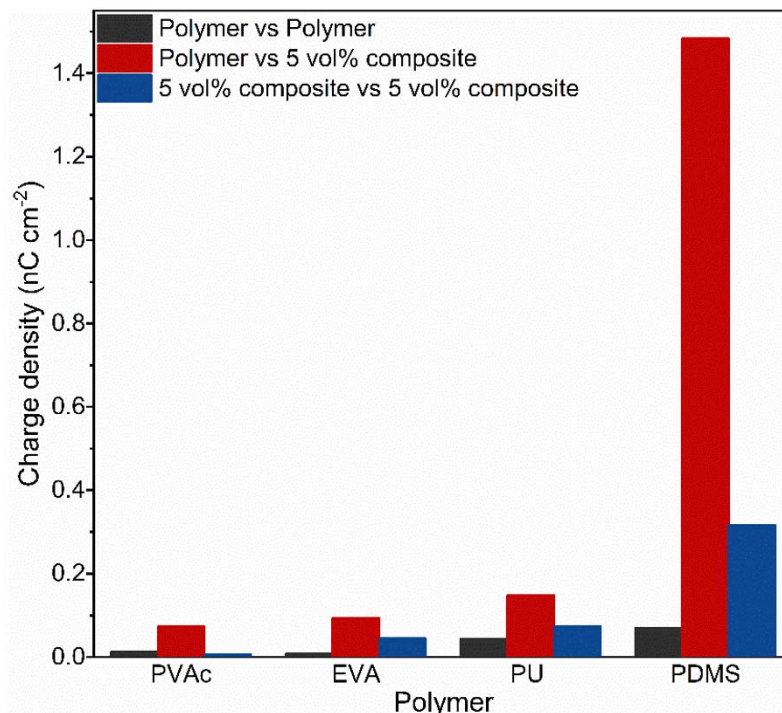
Fig. S4. Comparison of charge densities for polymers PVAc, EVA, PU and PDMS when their respective 5 vol% TiO_2 composites and pristine polymer layers are mutually contact-separated. When bare PDMS film is contact-separated with PDMS containing 5 vol% of TiO_2 nanoparticles 35 times higher current and voltage peaks are observed in comparison with TENG device based on identical bare PDMS films. The calculated charge increases for an order of magnitude from 0.07 nC cm^{-2} to 1.48 nC cm^{-2}. However, 5 vol% was the maximum content of nanoparticles that could be mixed in the PDMS to retain its crosslinking ability. The same effect was observed for PU.
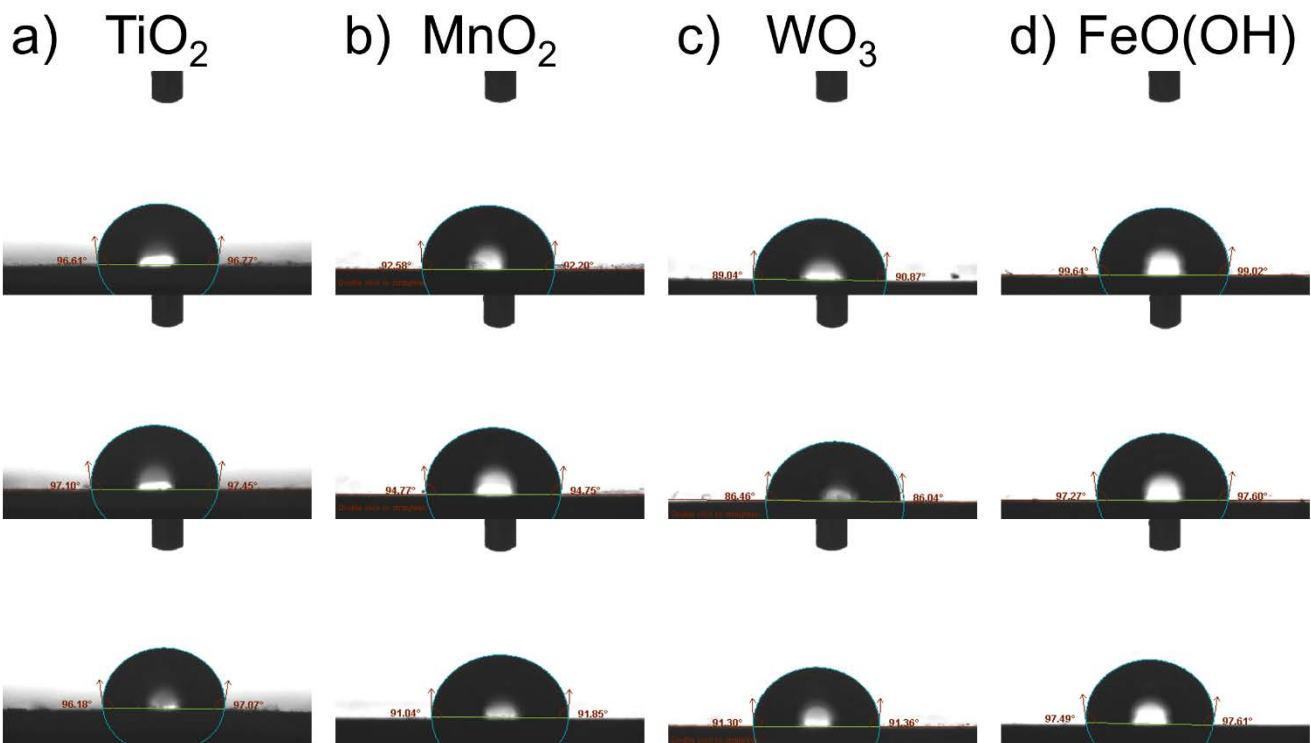
Fig. S5. Water contact angle (CA) measurements for EVA composites with (a) TiO_2, (b) MnO_2, (c) WO_3 and (d) FeO(OH) particles as fillers. To evaluate reliable CA values, each composite was measured three times at different surface locations.
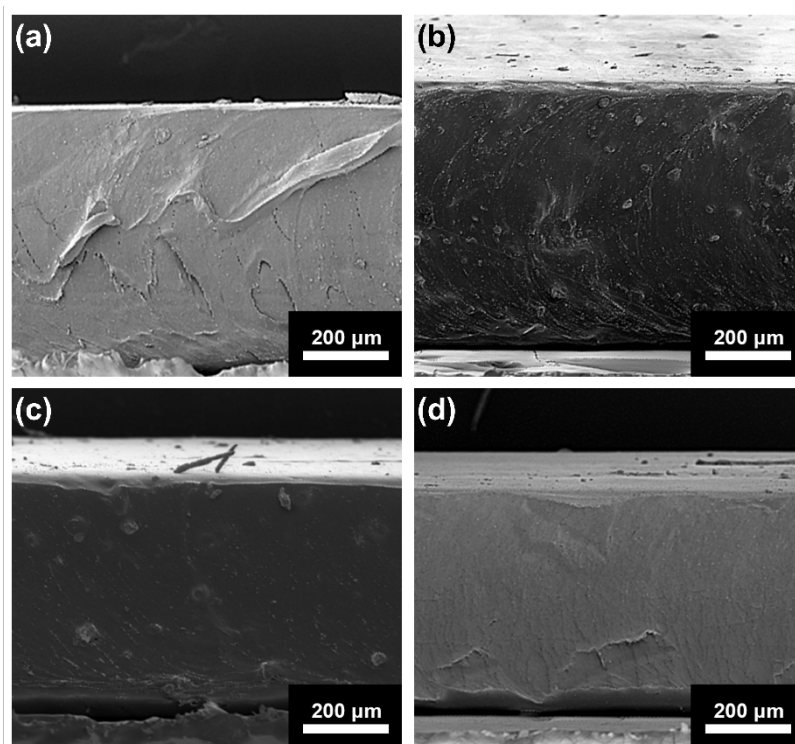
Fig. S6. (a) SEM image of EVA/TiO_2 (5 vol%) composite, (b) EVA/WO_3 (5 vol%) composite, (c) EVA/FeO(OH) (5 vol%) composite, (d) EVA/MnO_2 (5 vol%) composite.
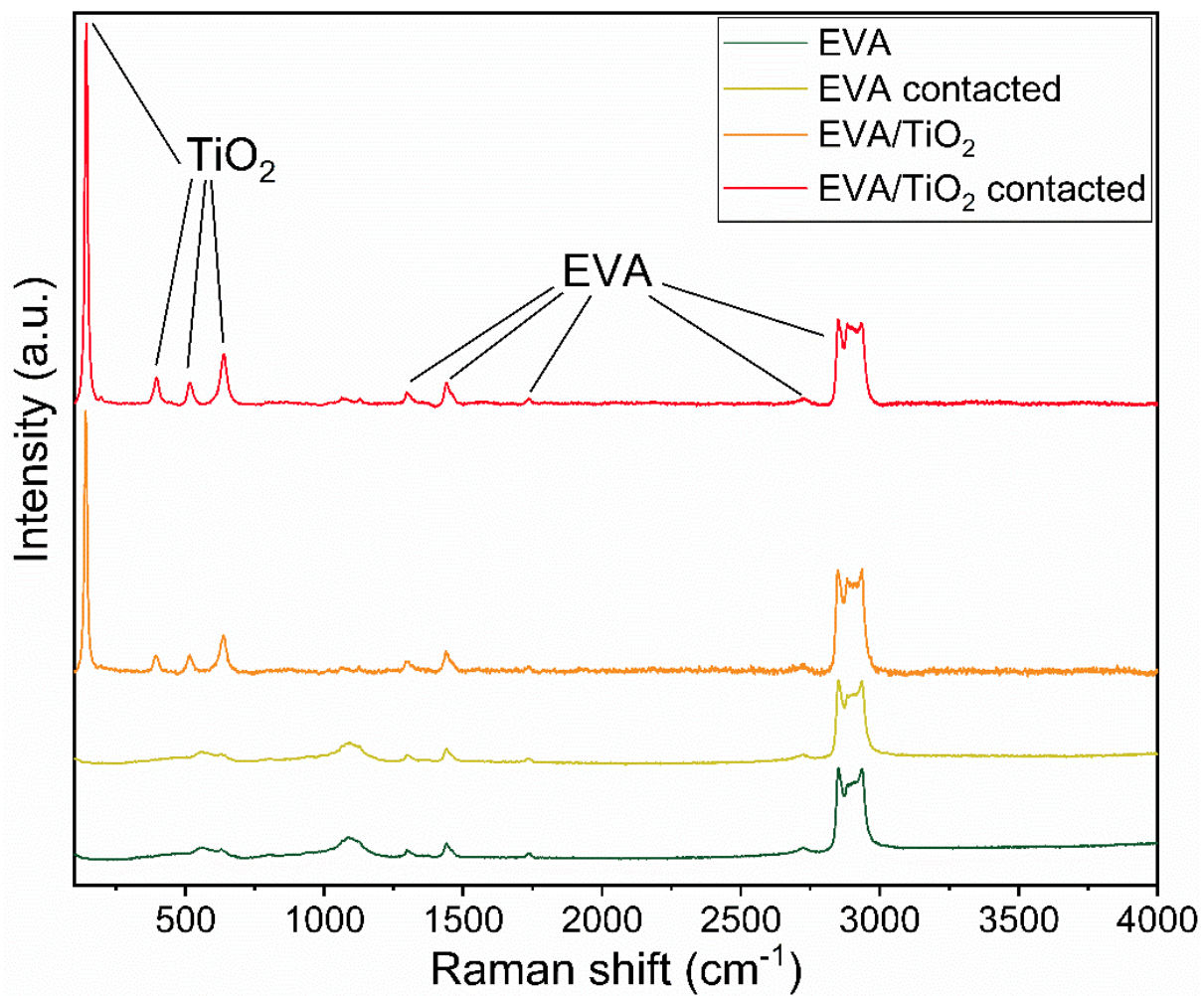
Fig. S7. Raman spectra of the pristine EVA and the EVA/TiO$_2$ (5 vol%) composite before and after triboelectric charging (EVA versus EVA/TiO$_2$) with 10000 contact-separation cycles.
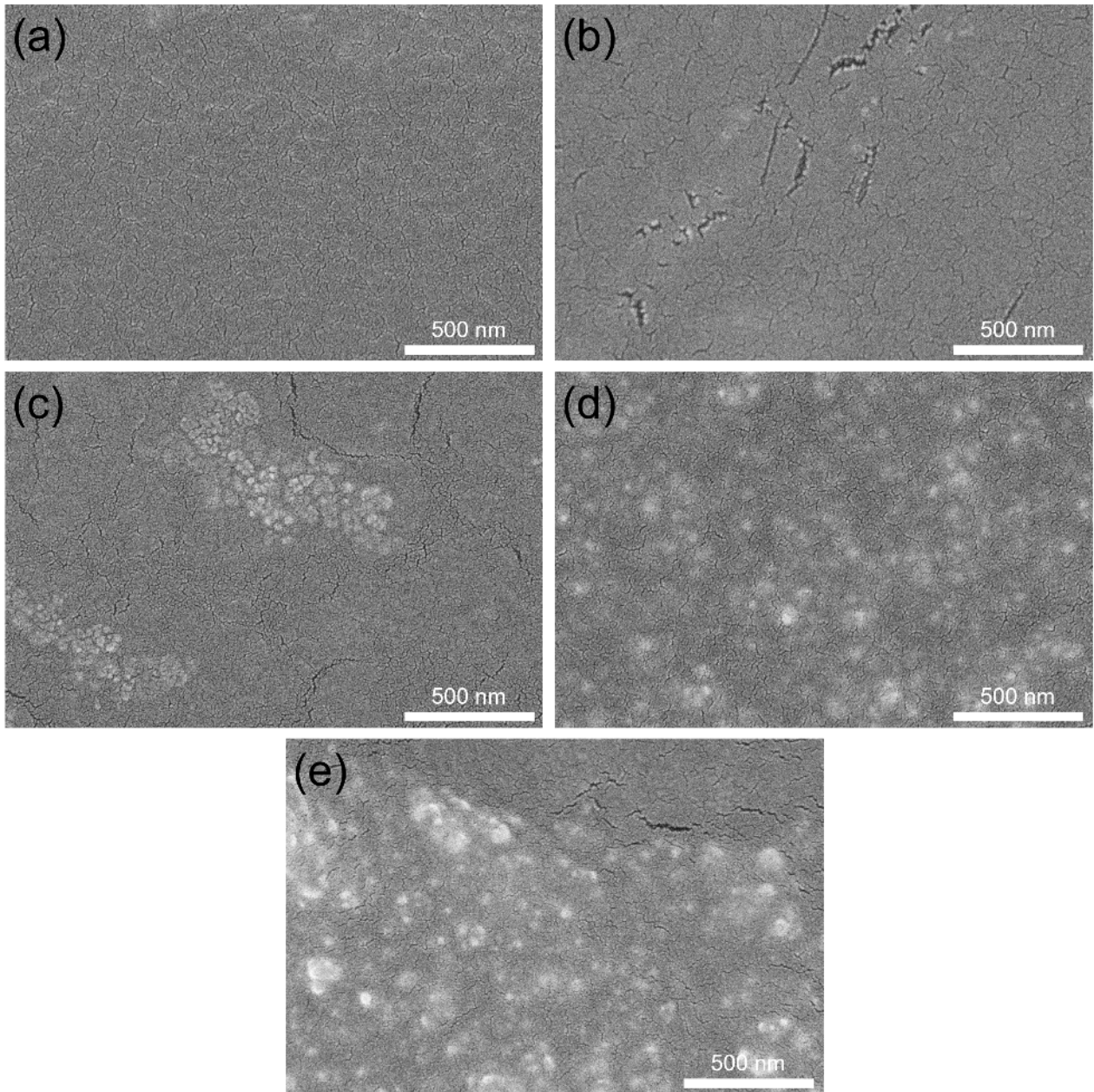
Fig. S8. Top-view surface SEM images of (a) EVA, (b) EVA/TiO$_2$ (2.5 vol%) composite, (c) EVA/TiO$_2$ (5 vol%) composite, (d) EVA/TiO$_2$ (10 vol%) composite and (e) EVA/TiO$_2$ (15 vol%) composite. Although the amount of the shadow of particles is different in each image, there is almost no deviation in the surface roughness due to the hot-pressing method and relatively small volume percentage (below ~15 vol%).
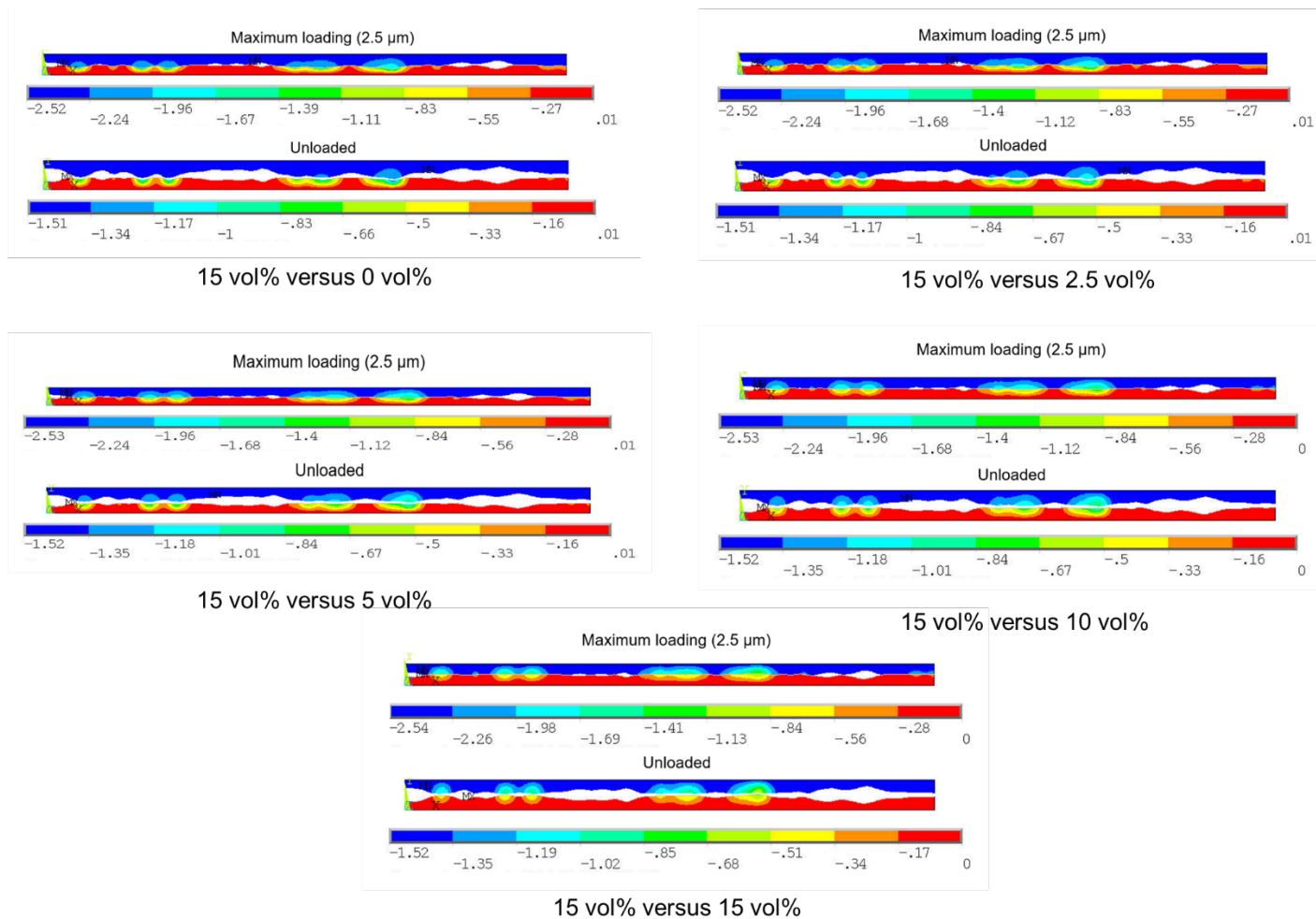
Fig. S9. Enlarged versions of main Fig. 5c-g to help readers' understanding and intuition.
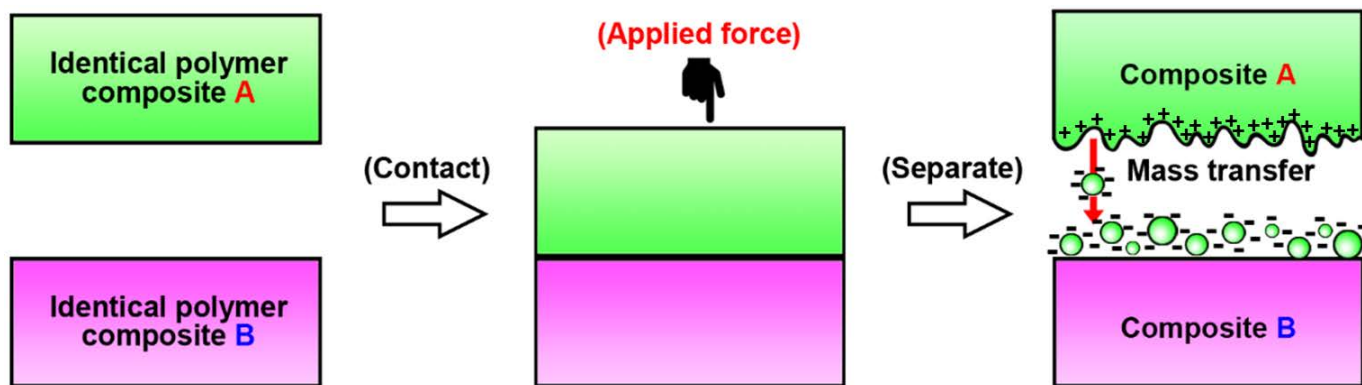
Fig. S10. Simplified schematics of mass (materials) transfer mechanism of polymer triboelectrification by heterolytic scissions. For the sake of simplicity, the mass transfer is expressed by one-directional and negatively-charged mass. In real cases, it can be bidirectional and both-charged mass by heterolytic cleavage of polymers.

Table S1. Surface length f, surface deformation Δ_f (%) and deformation ratio of surfaces used in simulations when maximum loading (2.5 µm displacement) conditions are applied.

Simulation	Surface	Initial f_0, µm	Max loading $f_{i(max)}$, µm	$\Delta_f = \frac{(f_0 - f_{i(max)})}{f_0} \times 100,\ \%$	Ratio of total deformations of 15 vol% layer and counterpart layers
15 vs 15 vol%	15 vol%		60.28	3.102	1
	15 vol%		60.28	3.102	
15 vs 10 vol%	15 vol%		60.36	2.974	1.032
	10 vol%		60.3	3.070	
15 vs 5 vol%	15 vol%	62.21	60.43	2.861	1.039
	5 vol%		60.36	2.974	
15 vs 2.5 vol%	15 vol%		60.58	2.620	1.061
	2.5 vol%		60.48	2.781	
15 vs 0 vol%	15 vol%		60.72	2.395	1.074
	0 vol%		60.61	2.572	

Table S2. Surface length f, surface deformation Δ_f (%) and deformation ratio of surfaces used in simulations when they are unloaded from maximum loading condition.

Simulation	Surface	Max loading $f_{i(max)}$, µm	Unloaded $f_{i(unload)}$, µm	$\Delta_f = \frac{(f_{i(max)} - f_{i(unl)})}{f_{i(max)}} \times 100,\ \%$	Ratio of total deformations of 15 vol% layer and counterpart layers
15 vs 15 vol%	15 vol%	60.28	60.76	0.796	1
	15 vol%	60.28	60.76	0.796	
15 vs 10 vol%	15 vol%	60.36	60.95	0.977	2.456
	10 vol%	60.3	60.54	0.398	
15 vs 5 vol%	15 vol%	60.43	61.14	1.175	5.066
	5 vol%	60.36	60.5	0.232	
15 vs 2.5 vol%	15 vol%	60.58	61.42	1.387	13.977
	2.5 vol%	60.48	60.54	0.099	
15 vs 0 vol%	15 vol%	60.72	61.62	1.482	12.834
	0 vol%	60.61	60.68	0.115	